MITSUBISHI ELECTRIC RESEARCH LABORATORIES
https://www.merl.com

AssemblyBench: Physics-Aware Assembly of Complex Industrial Objects

Li, Danrui; Zhang, Jiahao; Egger, Bernhard; Chatterjee, Moitreya; Lohit, Suhas; Marks, Tim K.; Cherian, Anoop

TR2026-076 June 04, 2026

Abstract

Assembling objects from parts requires understanding multimodal instructions, linking them to 3D components, and predicting physically plausible 6-DoF motions for each as- sembly step. Existing datasets focus on simplified scenarios, overlooking shape complexities and assembly trajectories in industrial assemblies. We introduce AssemblyBench, a synthetic dataset of 2,789 industrial objects with multi- modal instruction manuals, corresponding 3D part models, and part assembly trajectories. We also propose a transformer-based model, AssemblyDyno, which uses the instructional manual and the 3D shape of each part to jointly predict assembly order and part assembly trajectories. AssemblyDyno outperforms prior works in both assembly pose estimation and trajectory feasibility, where the latter is evaluated by our physics-based simulations.

IEEE Conference on Computer Vision and Pattern Recognition (CVPR) 2026

Mitsubishi Electric Research Laboratories, Inc.
201 Broadway, Cambridge, Massachusetts 02139

AssemblyBench: Physics-Aware Assembly of Complex Industrial Objects

Danrui Li[1*] Jiahao Zhang[2*] Bernhard Egger[3]
Moitreya Chatterjee[4] Suhas Lohit[4] Tim K. Marks[4] Anoop Cherian[4]
[1]Rutgers, The State University of New Jersey, USA [2]The Australian National University, Australia
[3]Friedrich-Alexander-Universität Erlangen-Nürnberg, Germany [4]Mitsubishi Electric Research Laboratories (MERL), USA
[1]danrui.li@rutgers.edu [2]jiahao.zhang@anu.edu.au [3]bernhard.egger@fau.de [4]{chatterjee,slohit,tmarks,cherian}@merl.com

https://merl.com/research/highlights/assemblybench

Abstract

Assembling objects from parts requires understanding multimodal instructions, linking them to 3D components, and predicting physically plausible 6-DoF motions for each assembly step. Existing datasets focus on simplified scenarios, overlooking shape complexities and assembly trajectories in industrial assemblies. We introduce AssemblyBench, a synthetic dataset of 2,789 industrial objects with multimodal instruction manuals, corresponding 3D part models, and part assembly trajectories. We also propose a transformer-based model, AssemblyDyno, which uses the instructional manual and the 3D shape of each part to jointly predict assembly order and part assembly trajectories. AssemblyDyno outperforms prior works in both assembly pose estimation and trajectory feasibility, where the latter is evaluated by our physics-based simulations.

1. Introduction

Assembling objects from constituent parts is a challenging yet ubiquitous task with substantial potential for automation, and it has myriad applications from household furniture assembly to large-scale manufacturing of complex industrial objects. As a result of the advancements in large vision-and-language models and robotics foundation models, the problem of object assembly has garnered significant interest recently in both the computer vision and robotics communities [16, 30, 33, 35, 43]. State-of-the-art approaches to address this task mainly consider IKEA-style furniture assembly, due to the availability of abundant collections of well-designed instruction manuals that detail each step of the process using language-free diagrams [35, 38, 43]. Furthermore, to facilitate assembly by inexperienced users, furniture parts are typically designed to be easily distinguishable, clearly illustrated in diagrams, and straightforward to attach to each other. Thus, datasets derived from such furniture assemblies offer a simplified yet useful setup to study this complex reasoning task.

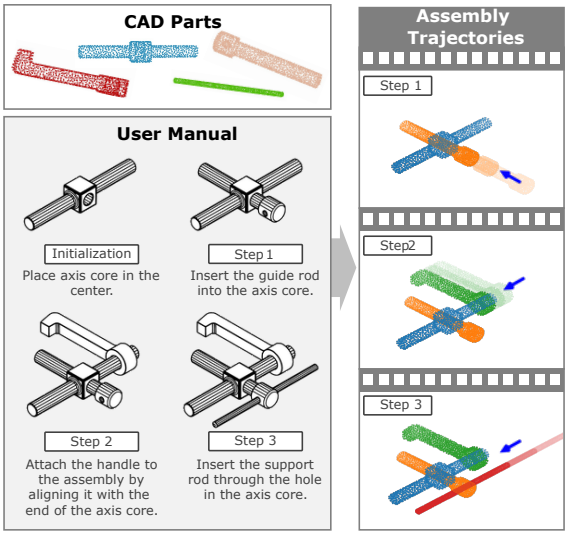

Figure 1. Given a step-wise manual with diagrams and text (*lower left*), we aim to assemble the corresponding set of 3D parts (*upper left*) in a virtual environment, outputting its step-wise assembly trajectories, which can be rendered into 4D animations (*right*).

However, furniture assemblies alone may not capture the full spectrum of complexities in real-world assembly processes, especially the process of moving assembly parts. For example, the assembly of electrical appliances (*e.g.*, air conditioners, ceiling fans, laundry machines), industrial equipment (*e.g.*, motors, gear boxes, hydraulic pumps), or even simple interactive toys. These objects often contain parts with complex geometries, and they may require sophisticated maneuvers such as insertion with twisting to assemble. While there have been several attempts at capturing varied aspects of this complex problem—*e.g.*, assembly from diagram-based instruction manuals [34, 35, 43], planning for robotic assembly [30, 33], and learning from video

*Work done during internships at MERL.

demonstrations [1, 19, 42]—there is a need for datasets that capture more of the common challenges in assembly.

Toward this end, we present AssemblyBench, a novel synthetic assembly dataset. It consists of nearly 3K assemblies spanning several categories of objects (not merely furniture) and featuring industrial objects. In contrast to prior non-IKEA datasets [32, 43], AssemblyBench extends the dataset modalities from assembled shapes to a set of CAD parts, step-by-step instruction diagrams with text descriptions, and assembly motion trajectories. Moreover, we introduce a pipeline that can be generalized for automatic instruction manual creation for any type of industrial objects from their CAD assemblies, which are commonly provided in mechanical design specifications.

To address the challenges in AssemblyBench, we present *AssemblyDyno*, a novel transformer-based architecture that predicts the assembly order of the parts as well as their 6-DoF motion trajectories. Specifically, AssemblyDyno is trained to learn a soft attention between the order of the instructions and the 3D part point clouds (encoded using a point cloud encoder) to regressing a discrete sequence of $SE(3)$ transformations for each part, along which the part should move in order to successfully complete its assembly. The entire set of motion sequences is jointly predicted by AssemblyDyno in a single forward pass. Our model is trained in a supervised setting, using ground-truth sequences of part trajectories, by minimizing chamfer-distance-based losses that account for invariance to symmetries in the parts' geometries.

In addition to utilizing the standard metrics for evaluating the performance of prior works on AssemblyBench (*e.g.*, symmetric chamfer distance and final success rate), we present a novel evaluation that executes the predicted part motion trajectories in a physics simulator [22] to verify their physical feasibility. Our key insights are three fold: i) while our training scheme does not include the simulator-in-the-loop, our supervised training might implicitly capture the physical constraints for assembly; ii) although instruction manuals are usually created to follow physically plausible part assembly, there may be other, novel motion pathways that could lead to a correct assembly; and iii) there may be inaccurate or physically infeasible steps in the predicted assembly that cannot be identified unless executed under physical constraints. For example, a predicted motion may cause the part to get stuck in an intermediate position, which would prevent the remainder of the assembly from proceeding. While prior protocols measure success using only the point-cloud alignment of the predicted final assembly, our physics-simulator-based evaluation offers a complete verification of the part assembly order, motion trajectories, and physical realizability, bringing successful assemblies significantly closer to real-world enactment.

We present extensive experiments demonstrating various aspects of AssemblyBench using AssemblyDyno. We find that a state-of-the-art baseline [43], which demonstrates nearly 60% success rates on furniture datasets, does not perform nearly as well (nearly 30% worse) on our challenging new dataset. In contrast, AssemblyDyno, with its incorporation of both diagrams and text descriptions from the instruction manual, leads to 12% improvements in the success rate of final pose estimate. Furthermore, AssemblyDyno predicts the assembly trajectories with better physics feasibility. It achieves about 33% success rate in a physical simulator by referencing to diagrams and texts with a trajectory smoothing loss, while the baseline method achieves only around 3%.

In summary, our main contributions include:

- **Dataset:** AssemblyBench that includes complex industrial part assemblies with multi-modal user manuals and assembly trajectories, produced using a VLM-based generative pipeline.
- **Model:** AssemblyDyno, a generalized feed-forward model that takes in multi-modal assembly steps and 3D part point clouds, predicting the parts' assembly order, final poses, and 6 DoF assembly motion trajectories.
- **Evaluation:** A physics engine based protocol to evaluate the physical feasibility of predicted assembly trajectories, where AssemblyDyno shows state-of-the-art results.

2. Related Work

Assembly Datasets. A comprehensive assembly dataset should include diverse geometries and contact types, incorporate realistic physical interactions, be realizable in a physics simulator, and capture the full assembly process rather than only final poses. Existing shape datasets such as PartNet [21] and IKEA-based assembly datasets [1, 19, 34, 35, 38, 42, 43] have been widely used, with IKEA manuals providing canonical step-by-step diagrammatic supervision. However, these datasets include a limited set of furniture objects with similar part geometries and lack kinematic constraints. Broader datasets covering toys [27] or electronics [29], as well as datasets with real-world video annotations [8, 27, 29, 45], broaden category coverage but still focus mainly on high-level goals or final part poses.

Motivated by these limitations and following [32], we build on the Assemble-Them-All (ATA) dataset [31, 32], which contains nearly 5K industrial CAD models with explicit part-insertion relations and physics-based disassembly trajectories [31]. Prior work has used ATA [32, 46], but it lacks step-by-step manuals, standardized part/trajectory representations, curated splits, and evaluation protocols.

Recent efforts aim to reduce manual annotation cost via automatic manual-generation pipelines, including parametric systems [24, 25, 37] and VLM-based dataset enrichment [11, 15, 41]. CheckManual [20] further explores VLM-driven operation-manual generation. How-

ever, assembly involves multi-part interactions, occlusions, and nontrivial 3D insertions, making manual generation substantially more challenging. Consequently, most datasets [5, 38, 43] provide only final part poses, overlooking the trajectories required for complex assemblies. Our dataset and pipeline address these gaps by producing standardized representations, full assembly trajectories, and step-by-step manuals. See Table 1 for detailed comparison.

Assembly Step Prediction. There are numerous works that attempt to predict assemblies without manuals [17, 18, 26, 40]. However, given the joint discrete-and-continuous search space for finding the part to assemble and generating its assembly trajectory, it is usually difficult for such methods to generalize. There are are also several recent works that use guidance from: i) final object renderings [16, 39, 46], ii) from step-wise manuals [34, 35, 43], or iii) assembly videos [19, 42], but mostly for IKEA-type furniture. Classical motion planning methods (e.g., RRT [14] and PRM [9]) have been explored for assembly via generating the motion trajectory from a predicted final part pose [46], including incorporating physical constraints [31, 32]. However, they are computationally expensive and require precise characterization of the physical constraints in the environment [12]. Thus, while we use a physics-based planner [31, 32] when generating our dataset, our model is trained in a supervised manner on the trajectories, implicitly learning the physics. Further, our use of a single forward pass to predict all assembly steps at once in discrete time steps is computationally efficient and robust.

3. Proposed Method

In its generalized form, an assembly task involves understanding the procedure from instruction manuals, identifying the object parts to be assembled at each step, and executing the assembly steps as depicted in the manual to fit the parts together following physically feasible motion paths. Following this recipe, we formulate our task as follows.

We are given an unordered set of N assembly parts as 3D point clouds $\{P_i\}_{i=1}^{N}$, with each part assumed to contain the same number of points), and a manual consisting of a sequence of assembly instructions denoted $(\mathcal{I}_1, \cdots, \mathcal{I}_N)$, where each step involves adding one part. Our objective is to have a model that: i) predicts the assembly order by grounding the 3D parts to their instructions, i.e., producing part indices $(\hat{\pi}_1, \hat{\pi}_2, \cdots, \hat{\pi}_N)$ such that the part $\mathcal{P}_{\hat{\pi}_i}$ is associated with instruction $\mathcal{I}_i$, and ii) predicting the part motion trajectories for each assembly step as $\big((\hat{R}_i^k, \hat{t}_i^k) \in \mathrm{SE}(3)\big)$, where $i \in \{1, \ldots, N\}$ represents the assembly step number, and $k \in \{1, \ldots, T\}$ represents the time step within a part's trajectory. The number of parts N is assumed to vary across objects, however the number of time steps T in each part's assembly trajectory is considered fixed. Each instruction step $\mathcal{I}_i$ in the manual consists of a diagram illustrating the assembly step and a free-form text description detailing the step. We use 2D line-drawing diagrams similar to IKEA manuals, showcasing 3D parts without textures in a fixed parallel projection. The assembly trajectory in assembly step i is represented as a sequence of T 6-DoF poses, $\big(\hat{R}_i^k, \hat{t}_i^k\big)$, which respectively represent the 3×3 rotation matrix and 3×1 translation vector of the part at the kth time-step of its trajectory. In our experiments, we use $T = 12$ for the number of time-steps.

This work requires us to implement three parts: i) building the AssemblyBench dataset using an automatic annotation pipeline, which adheres to the assembly process described above while incorporating complex assemblies (detailed in § 3.2); ii) proposing a novel transformer-based reasoning model, AssemblyDyno, which predicts an entire 3D assembly process from an instruction manuals (described in § 3.3); and iii) proposing a set of evaluation metrics that evaluates the entirety of the assembly performance (explained in § 3.4).

3.1. AssemblyBench Dataset

AssemblyBench contains multimodal instruction manuals for 2789 assemblies in total, covering a wide range of categories including furniture, appliances, and mechanical components. Each manual provides the 3D mesh and point cloud of each individual part, as well as step-wise assembly instructions consisting of diagrams and text. The number of steps (i.e., the number of parts) for each assembly ranges from 2 to 20, with an average of 6.7 steps on average. Table 1 contrasts AssemblyBench with prior datasets proposed for assembly-related tasks. As is clear, AssemblyBench generalizes prior works while including ground-truth part assembly trajectories, exhibiting a variety of motion patterns. In Figure 2, we provide detailed statistics on the properties of our dataset. Out of all of the trajectories, 5.84% involve rotational movements such as sophisticated twists, 5.42% involve long translation movements that indicate insertions into a hole or slot, and there are about 58 parts that need long distance insertions combined with rotations for the assembly. We divide the set of 2789 assemblies into train/val/test splits in 80%-10%-10% allocation.

3.2. AssemblyBench Construction Pipeline

The following subsections present our automatic data generation pipeline of AssemblyBench, illustrated in Figure 3. We note that our pipeline is very general and could be used to generate assembly instruction manuals for a broad variety of objects, given only an object's 3D CAD model. Such CAD models of assembled real-world objects are widely available (e.g., from machine designs).

Part Order and Motion Trajectories: There are two important sub-tasks in assembly: i) deciding the order of the parts to select for the assembly (so that it is physically re-

Table 1. Comparison of assembly/manipulation datasets. Legends: diagrams, text instructions, videos, 3D objects.

Work	Domain	Input	Output	Size
IKEA-Manual [38]	Furniture	,	Assembly order, 6D part pose	102
IKEA-Manuals-at-Work [19]	Furniture	, ,	6D part pose, temporal alignments	36
ProMQA-Assembly [5]	Toys	, ,	Assembly order, General QA	78
LEGO-VLM [7]	Modular toy bricks	, ,	Object localization, state judgement	65
MEPNet [37]	Modular toy bricks	,	Assembly order, part pose	8000
ManualPA [43]	Furniture	,	Assembly order, 6D part pose	6871
CheckManual [20]	Appliances	, ,	Manipulation plan, action trajectory	369
Manual2Skill++ [34]	Furniture, toys, industrial	,	Assembly order, 6D pose trajectories	20+
AssemblyBench (Ours)	All the above except toy bricks	, ,	Assembly order, 6D pose trajectories	2789

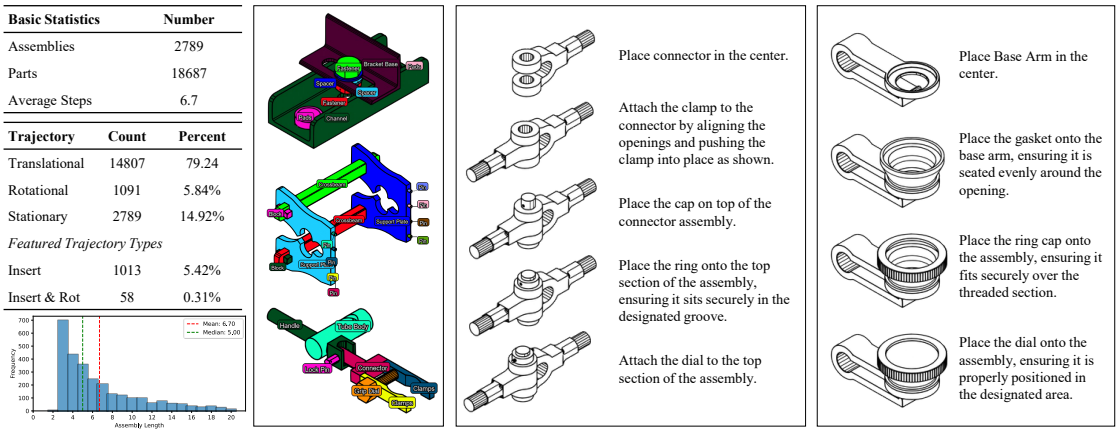

Distribution of Step Number | Generated Part Names | User Manual Example (ID: 2788) | User Manual Example (ID: 7869)

Figure 2. **Overview of AssemblyBench**. *Column 1:* Statistics of our AssemblyBench dataset and histogram of the number of parts per assembly in AssemblyBench. *Column 2:* Generated part names in AssemblyBench. The coloring and the labels are for visualization in this figure only—they are not included in the model inputs. *Columns 3–4:* Example generated instruction manuals for two different assemblies.

alizable) and ii) planning the motion of each part from its initial pose to the final assembled pose. The assembly-by-disassembly process [31, 32] tackles these sub-tasks via importing the 3D CAD models into a physics engine. Specifically, it uses a depth-first-search algorithm to attempt to disassemble the object one part at a time via applying forces along the part axes, until the part becomes disassociated from the other parts. This scheme discovers a disassembly sequence that includes both a disassembly order of parts and a 6-DoF pose trajectory for removing each part. Reversing both of these yields both the assembly part order and the assembly pose trajectories. To create AssemblyBench, we import each CAD object's assembly steps and motion trajectories (discretized to T time steps) to Blender [6] and format them to produce assembly animations.

Diagram Generation: A key ingredient in the assembly process is the instruction manual, which any robotic platform intended to do assembly tasks must be equipped to follow for safety and physical feasibility. In AssemblyBench, for each assembly step and each camera view, we render the diagram using Blender as follows. First, we use a line-art style without coloring to mimic the visual style in real-world instruction manuals such as IKEA's. Then, we use the CAD part position at the final time step of the trajectory to represent the part's final assembled state. We also render a segmentation map of this diagram for later text annotations.

We render the diagrams using a fixed set of isometric camera views. The diagrams from multiple camera views are used in two ways. First, they are selected in the later text annotation stage as the reference materials for a large vision-and-language model (VLM), as detailed later. Second, they are used to choose the camera view for the instruction manual, which uses a fixed camera view throughout all assembly steps (see Supplementary Material for details).

Instructional Text Generation:

To construct AssemblyBench, we generate text instructions to accompany each diagram, forming realistic step-by-step manuals. Our pipeline has two stages. First, we prompt a VLM (GPT-4.1) with diagrams of all individual parts to assign consistent names (e.g., "fastener", "wire frame"), ensuring uniform terminology throughout the manual. Second, using these names, we prompt the VLM to produce textual instructions for each assembly step based on that step's diagram.

Because our industrial assemblies contain complex shapes, frequent occlusions, and repeated part types (e.g.,

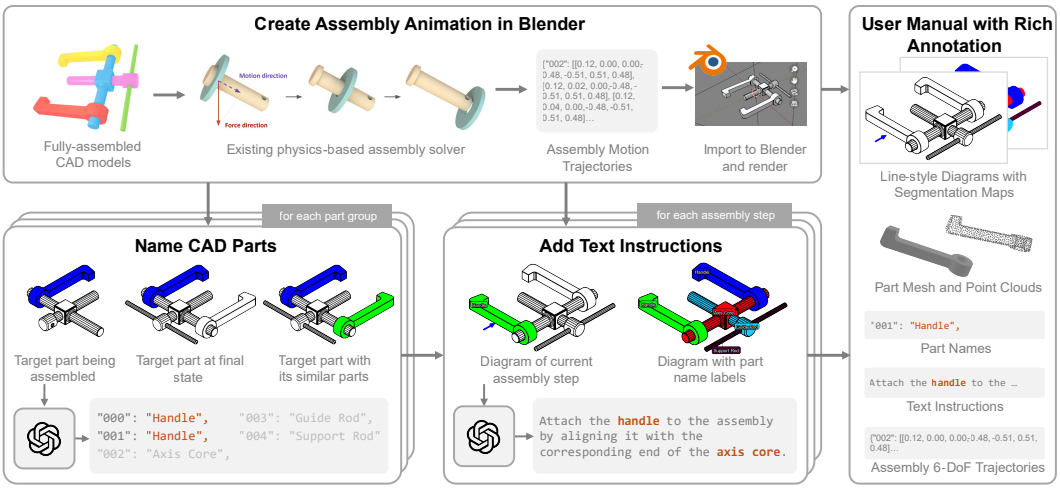

Figure 3. **Manual creation pipeline for AssemblyBench**. *Top left:* From a CAD model of an assembled object, we calculate the part assembly trajectories using a physical engine and import the animations to Blender. *Bottom left:* Blender renderings are fed to VLMs to create CAD part names and textual assembly instructions. *Right:* All annotations are used to generate a single step in the final manual.

multiple identical screws), obtaining consistent part names from a single camera view is challenging. Parts may be hidden in later steps (temporal occlusion), blocked from view (spatial occlusion), or duplicated. To address these issues, we apply several visual prompting techniques (described in the Supplementary Material). After generating consistent part names (see Fig. 2), we produce the step-by-step instructions by providing the VLM with: (i) the current step's diagram with the target part highlighted, and (ii) the same diagram with all parts color-coded and labeled. This ensures consistent naming across all assembly steps (see "Add Text Instructions" in Fig. 3).

3.3. AssemblyDyno: Our Assembly Model

As shown in Figure 4, the input to AssemblyDyno is a step-by-step instruction manual and the corresponding set of separated 3D part point clouds. Our model starts with multimodal encoders, converting each instruction step and each part's point cloud into feature embeddings of the same dimension D. After using an existing predictor to obtain part orders in the form of a permutation matrix, we apply a transformer decoder with positional encodings to predict the assembly trajectory for each step, as explained below.

Feature Extraction: We begin by applying off-the-shelf encoders to obtain semantic latent features from the inputs. For the 3D part point clouds $\{\mathcal{P}_i\}_{i=1}^{N}$, we use a lightweight PointNet variant [2], similar to that in [16, 43]. For the sequence of step diagrams $(I_j^{\text{img}})_{j=1}^{N}$, since the assembly instructions progress incrementally, we focus on the differences between successive steps. For any pair of consecutive diagrams $\mathcal{I}_j^{\text{img}}$ and $\mathcal{I}_{j+1}^{\text{img}}$, $j \in \{1, 2, \ldots, N-1\}$, we form a difference image $|\mathcal{I}_j^{\text{img}} - \mathcal{I}_{j+1}^{\text{img}}|$ that highlights the newly added part relative to the partially assembled object. This difference image is then divided into K patches and passed through a DINOv3 image encoder [28] to extract features. For the corresponding text content, we use the Qwen-3 embedding model [44] with frozen model weights. Each of the three modalities is projected to the same feature dimensionality D using linear layers, yielding part features $f^{\mathcal{P}} \in \mathbb{R}^{N\times D}$, image features $f^{\text{img}} \in \mathbb{R}^{N\times K\times D}$, and text features $f^{\text{txt}} \in \mathbb{R}^{N\times D}$. To fuse image and text features into one feature, we concatenate the two features by repeating text features along the patch dimension and apply linear projections, yielding instruction features $\mathbf{f}^{\mathcal{I}} \in \mathbb{R}^{N\times K\times D}$.

Predicting Part Assembly Order: Applying a similar approach as Manual-PA [43], we calculate a similarity matrix between the embeddings of the parts and those of the instructions with a max-pooling operation on patch dimension K. Then, we use the Hungarian matching algorithm [13] to convert the similarity matrix into the predicted order $(\hat{\pi}_1, \hat{\pi}_2, \cdots, \hat{\pi}_N)$, which is projected into a permutation matrix $M \in \{0,1\}^{N\times N}$.

Predicting Assembly Trajectories: To perform part-to-part interactions, we add the permutation matrix M with positional encoding [36] to the part features f^P and send the results to a self-attention transformer decoder. Then, we feed the outputs to a cross-attention module with temporal dimension, where position-encoded instruction features are added to produce the latent feature of assembly trajectories, shaped as $\mathbb{R}^{N\times T\times D}$. Finally, the latent feature is converted into a sequence of poses $\left(\{\{(\hat{R}_i^k, \hat{t}_i^k)\}_{k=1}^{T}\}_{i=1}^{N}\right)$ using a pose prediction head [43], where the rotations are represented using quaternions.

Training Losses: We train one model with the above architecture for part order prediction, and a second model with the same architecture for trajectory prediction. During trajectory prediction learning, we always feed the model using the ground-truth part order.

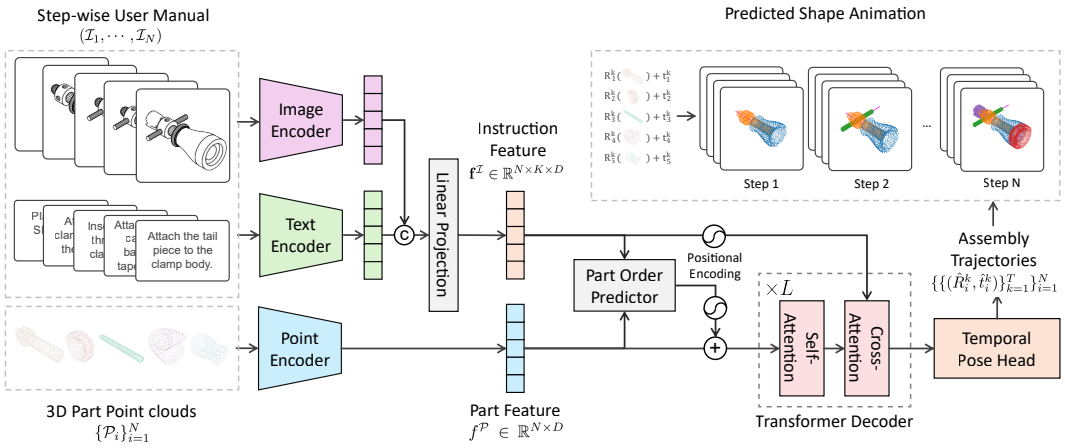

Figure 4. **Model Architecture of AssemblyDyno**. (1) Feature Extraction: AssemblyDyno starts with multi-modal encoders, converting user manual instructions and 3D part point clouds into embeddings of the same feature dimension D. (2) Predict Part Order: we use an existing predictor to get part order in the form of a permutation matrix. (3) Predict Assembly Trajectories: we use a transformer decoder with positional encodings to predict the assembly trajectory for each step.

Loss for Order Prediction: We optimize the similarity matrix between the instruction features $f_j^{\mathcal{I}}$ and part features $f_{\sigma(i)}^{\mathcal{P}}$. In the similarity matrix, a correct match between $f_j^{\mathcal{I}}$ and $f_{\sigma(i)}^{\mathcal{P}}$ yields a higher value. Based on this motivation, we adopt an InfoNCE loss [4, 23] design:

$$\mathcal{L}_{\text{order}} = -\frac{1}{B}\sum_{i=1}^{B}\log\frac{\exp\Big(\text{sim}(\mathbf{f}_{\sigma(i)}^{\mathcal{P}}, \mathbf{f}_i^{\mathcal{I}})/\tau\Big)}{\sum_{j=1}^{B}\exp\Big(\text{sim}(\mathbf{f}_{\sigma(i)}^{\mathcal{P}}, \mathbf{f}_j^{\mathcal{I}})/\tau\Big)},$$

where B is the batch size, $\sigma(i)$ denotes a permutation over part indices, $\text{sim}(\cdot)$ computes the similarity between two features, and τ is a temperature scaling factor.

Loss for Trajectory Prediction:

Inspired by [16, 43], the point-cloud loss $\mathcal{L}_P$ measures the difference between the point clouds of the predicted final assembly at step T (all parts in their final poses) and the ground-truth assembly.

$$\mathcal{L}_P = \text{CD}\left(\bigcup_{i=1}^{N}(\hat{R}_i^{(T)}P_i + \hat{t}_i^{(T)}),\ \bigcup_{i=1}^{N}(R_i^{(T)}P_i + t_i^{(T)})\right),$$

where $\bigcup_{i=1}^{N}$ represents the union of all N transformed parts to form the complete assembled shape, and $\text{CD}(\cdot)$ denotes the bidirectional chamfer distance, which measures the difference between two point clouds [3].

In addition to the overall point-cloud loss, we separately measure translation and rotation losses. For translation loss,

$$\mathcal{L}_T = \frac{1}{NT}\sum_{i=1}^{N}\sum_{k=1}^{T}\|\hat{t}_i^{(k)} - t_i^{(k)}\|_2,$$

where $\hat{t}_i^{(k)}$ is the predicted translation at time step k, t_i is the ground-truth translation, and $\|\cdot\|_2$ denotes the ℓ_2 norm.

For rotational loss, as parts may have rotational symmetries, solely relying on ℓ_2 distance will miss some correct answers. So we use chamfer distance on the point clouds,

$$\mathcal{L}_R = \frac{1}{NT}\sum_{i=1}^{N}\sum_{k=1}^{T}\text{CD}(\hat{R}_i^{(k)}P_i, R_i^{(k)}P_i),$$

where $\hat{R}_i^{(k)}$ is the predicted rotation for part i at time step k, R_i is the ground-truth rotation, and $\text{CD}(\cdot)$ denotes the bidirectional chamfer distance between the rotated point clouds.

To encourage temporally smooth motions, we additionally regularize the frame-to-frame "velocity" of both translations and rotations of the predicted trajectories. We penalize the finite difference between consecutive frames,

$$\mathcal{L}_{S_T} = \frac{1}{N(T-1)}\sum_{i=1}^{N}\sum_{k=1}^{T-1}\left\|\hat{t}_i^{(k+1)} - \hat{t}_i^{(k)}\right\|_2^2, \quad (1)$$

$$\mathcal{L}_{S_R} = \frac{1}{N(T-1)}\sum_{i=1}^{N}\sum_{k=1}^{T-1}\left\|\hat{q}_i^{(k+1)} - \hat{q}_i^{(k)}\right\|_2^2. \quad (2)$$

The final loss is a weighted sum of all the components:

$$\mathcal{L} = \lambda_P\mathcal{L}_P + \lambda_T\mathcal{L}_T + \lambda_R\mathcal{L}_R + \lambda_{S_T}\mathcal{L}_{S_T} + \lambda_{S_R}\mathcal{L}_{S_R}. \quad (3)$$

3.4. Physics-Aware Evaluation in AssemblyBench

Our evaluation captures three aspects of assembly: if a model: i) correctly grounds each diagram to its part, ii) can make correct prediction of the final 3D poses of the parts (*Static Pose Estimate*), and iii) can predict 3D assembly trajectories that are physically feasible (*Assembly in Simulator*). For (i), we use the standard Kendall's Tau (KD) [10] metric to compute the correlation between the actual assembly order $(\pi_1, \pi_2, \cdots, \pi_N)$ and the predicted one $(\hat{\pi}_1, \hat{\pi}_2, \cdots, \hat{\pi}_N)$. For (ii), similar to prior works,

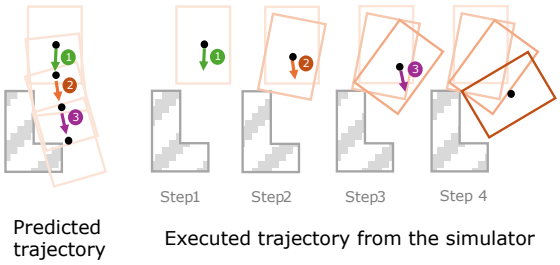

Figure 5. We use a physics simulator to execute the predicted assembly trajectory, evaluating whether it is physically feasible.

[16, 17, 43], we use the Shape Chamfer Distance (SCD), Part Assembly Correctness (PA), and Success Rate (SR). For (iii), we detail our new evaluation framework below.

As noted above, physical feasibility of predicted assembly trajectories is important for real-world adoption. In order to capture such feasibility, we propose to execute the predicted trajectories within a physics-based simulator to check their correctness. We use Newton Physics [22] as our simulator and evaluate the assembly process step-by-step: For each predicted step, we use the velocity sequence of the predicted trajectory as the control signal to roll out the simulation. Then we measure the difference between the simulation results and the ground truth.

Initially, we set up the parts that were assembled in previous steps of the instruction manual within the simulator, using their predicted final poses. Then we place the current part that is to be assembled, using the pose from the first time step of its predicted trajectory. We ignore gravity in this work for simplicity. Next, as shown in Figure 5, we let Δt represent the duration of each time step of the trajectory. Then we start the simulation by assigning v_1 as the initial velocity of the part and let the simulation run for Δt. The part might collide into other parts and change its velocity during that time step. After Δt, we iteratively assign v_2 and v_3 each for the same amount of time, and so on through to the final time step. The process is depicted in Figure 5.

We measure the prediction quality by comparing the executed pose trajectory from the simulator to the ground truth. Apart from using **PA** and **SR** in the simulation setting by following the same algorithms, we also present two new metrics to account for part symmetries. Specifically, due to the part symmetries and thus potential for non-unique solution poses, we do not compute the translation or rotational differences. Instead, we apply chamfer distance on two common trajectory evaluation metrics, i.e., ADE and FDE, resulting in the following variants:

- **Average Chamfer Distance (ACD)**: For each time step, we apply the corresponding executed pose and ground truth pose to the point clouds of their related parts and computes the chamfer distance between them. The chamfer distances from all time steps are averaged and the quartile values for all parts in all assemblies is reported.
- **Final Chamfer Distance (FCD)**: Similar to ACD, but instead of averaging over all time steps, we only take the chamfer distance of the final time step and report the median over all assemblies. We report the quartile values for all parts in all shapes.

4. Experiments

Table 2 provides a comprehensive evaluation of assembly trajectory prediction, final pose estimation, and full assembly simulation across multiple ablations. We compare AssemblyDyno to its ablations and to [43]. Since some baselines (e.g., [43]) do not predict trajectories, we generate them heuristically: from the predicted final pose, we translate the part outward from the object's center of mass (without rotation) for a distance equal to half the diagonal of its predicted bounding-box. Reversing this path yields the assembly motion.

Part Order and Final Pose: We first analyze the *GT part-order* setting, which serves as a sanity check to isolate the model's trajectory-prediction and pose-estimation capabilities from ordering errors. When provided with perfect part orders, AssemblyDyno consistently achieves the strongest performance across nearly all me trics. In the *Final Pose Estimate* block, AssemblyDyno attains the lowest SCD scores and the highest PA/SR values among the compared methods, highlighting its accurate trajectory reasoning and robust geometric understanding. In the *Assembly in Simulator* block, AssemblyDyno also yields superior PA and SR, even though the model is not trained with simulator feedback (see Figure 6). This demonstrates strong real-to-sim transfer of predicted motion trajectories. The ablation results further validate key model components: removing the text encoder (`w/o text`) or replacing the trajectory predictor with the naïve baseline (`w/o trajectory`) leads to consistent drops in PA, SR, ACD, and FCD, underscoring the importance of both textual grounding and the dedicated trajectory module.

We then analyze the *standard setting*, where the model must predict part orders before generating trajectories. Here, performance decreases across all methods, reflecting the substantial influence of ordering quality on downstream assembly outcomes. Despite this, AssemblyDyno still outperforms prior work, though the margin over its own ablations becomes smaller. This trend is especially visible in PA and SR, where the advantage of AssemblyDyno over `w/o text` narrows. We attribute this to two key factors: (1) assembly order prediction becomes the dominant bottleneck, and errors in ordering propagate into trajectory and pose predictions; and (2) textual information contributes limited additional signal for order prediction, since step-wise diagrams already strongly constrain the next operation, reducing the marginal benefit of language inputs at this stage. Overall, the table highlights three central insights: (i) our

Table 2. **Part assembly results on the test split of AssemblyBench**. We bold the best results and highlight the second best results in blue.

Model	Ordering	Final Pose Estimate			Assembly in Physics Simulator							
	KD↑	SCD(10^{-3})↓	PA(%)↑	SR(%)↑	ACD(10^{-3})↓			FCD(10^{-3})↓			PA(%)↑	SR(%)↑
					25%	50%	75%	25%	50%	75%		
Standard Setting												
AssemblyDyno	**0.819**	3.91	**71.21**	34.64	**6.95**	34.77	156.74	3.31	**15.97**	110.30	**42.76**	13.57
w/o text	0.805	**3.83**	70.28	**35.00**	6.99	**33.68**	**148.86**	**3.03**	17.25	**99.77**	41.77	**15.00**
w/o trajectory	**0.819**	4.42	67.63	30.00	104.73	188.94	317.76	11.95	58.52	199.64	22.09	1.43
ManualPA [43] (ICCV'25)	0.788	4.24	70.04	33.57	104.66	192.79	325.50	11.75	56.04	209.09	23.24	1.79
Use GT part orders												
AssemblyDyno	–	3.87	**79.69**	**44.29**	**3.23**	**9.97**	**29.74**	**1.50**	**4.43**	**12.41**	**70.15**	**33.57**
w/o text	–	**3.78**	78.19	42.86	3.45	10.77	35.28	1.61	4.85	14.32	67.96	31.79
w/o trajectory	–	3.80	79.31	43.21	136.48	235.16	390.23	6.90	37.39	197.65	29.85	3.57
ManualPA [43] (ICCV'25)	–	4.15	77.40	39.28	142.32	230.52	382.62	6.02	35.00	196.51	31.33	2.14

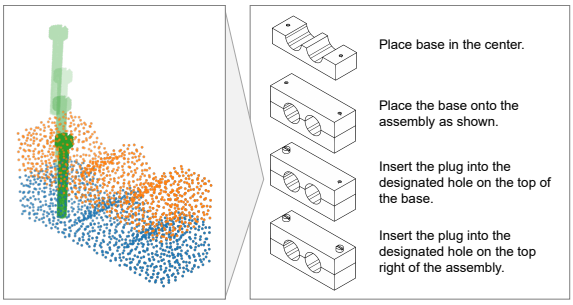

Figure 6. Given the instruction manual on the right, AssemblyDyno showcases the capability of predicting insertion assembly trajectory. Key frames of the trajectory are shown on the left.

model is intrinsically strong at pose and trajectory prediction, as shown by the GT-order results; (ii) the ablations validate the contributions of the text encoder and structured trajectory module; and (iii) in realistic deployment conditions, improving part-order prediction is crucial for unlocking further gains in downstream assembly performance.

Physics-based Evaluation:

We further show that our simulator-based evaluation provides a more stringent assessment of trajectory quality. Figure 7 compares the median translation errors of the *predicted* trajectories (orange) and the corresponding *simulated* trajectories (green). Although both decrease over time, the simulated error remains higher and the gap widens toward later frames, indicating that the simulator exposes compounding inaccuracies such as collisions or infeasible motions. Early in the trajectory, the simulated-error variance is larger because early-time-step predictions contains large variance that deviate substantially from ground truth. As the object approaches assembly, the physical constraints align more closely with the true configuration, reducing variance; however, these same constraints and obstacles still impede the predicted motion from reaching the final pose, resulting in a slightly higher but more stable residual error. Thus, the simulator-based metric offers a stricter and more realistic measure of trajectory feasibility.

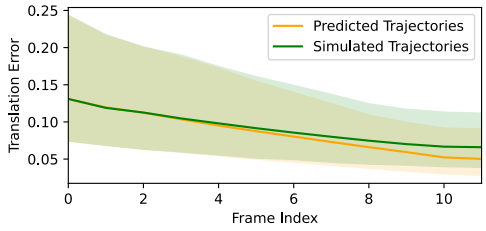

Figure 7. Median translation error with respect to ground truth as a function of trajectory frame. Shaded regions denote the 25th–75th percentiles computed across all object parts. The simulated trajectories exhibit consistently larger deviations due to collisions and other dynamic interactions, revealing hidden failure modes that are not captured when evaluating predictions alone.

5. Conclusion

We introduced AssemblyBench, a large-scale, multi-modal assembly dataset that extends beyond furniture to include complex industrial objects, complete with step-wise diagrams, textual descriptions, and ground-truth 6-DoF part trajectories. Building on this foundation, we presented AssemblyDyno, a unified transformer-based architecture that jointly predicts assembly order, final poses, and physically plausible motion trajectories. Our experiments demonstrate that existing state-of-the-art methods struggle on the richer and more challenging scenarios offered by AssemblyBench, while AssemblyDyno achieves substantially stronger performance in both final pose estimation and simulator-executed assembly. The analysis further highlights the benefits of integrating multi-modal manual information and structured trajectory prediction, as well as the importance of accurate order prediction for full assembly success. Overall, our work provides a comprehensive benchmark and modeling framework that brings instruction-guided assembly significantly closer to real-world applicability, with opportunities for future advances in order prediction, physical reasoning, and robotic execution.

Please see the supplementary material for more detailed results.

References

[1] Yizhak Ben-Shabat, Xin Yu, Fatemeh Saleh, Dylan Campbell, Cristian Rodriguez-Opazo, Hongdong Li, and Stephen Gould. The ikea asm dataset: Understanding people assembling furniture through actions, objects and pose. In *Proceedings of the IEEE/CVF Winter Conference on Applications of Computer Vision*, pages 847–859, 2021. 2

[2] R. Qi Charles, Hao Su, Mo Kaichun, and Leonidas J. Guibas. PointNet: Deep learning on point sets for 3D classification and segmentation. In *2017 IEEE Conference on Computer Vision and Pattern Recognition (CVPR)*, pages 77–85, 2017. 5

[3] Haoqiang Fan, Hao Su, and Leonidas J Guibas. A point set generation network for 3D object reconstruction from a single image. In *Proceedings of the IEEE conference on computer vision and pattern recognition*, pages 605–613, 2017. 6

[4] R. Hadsell, S. Chopra, and Y. LeCun. Dimensionality reduction by learning an invariant mapping. In *IEEE Computer Society Conference on Computer Vision and Pattern Recognition (CVPR)*, pages 1735–1742, 2006. 6

[5] Kimihiro Hasegawa, Wiradee Imrattanatrai, Masaki Asada, Susan Holm, Yuran Wang, Vincent Zhou, Ken Fukuda, and Teruko Mitamura. Promqa-assembly: Multimodal procedural qa dataset on assembly. *arXiv preprint arXiv:2509.02949*, 2025. 3, 4

[6] Roland Hess. *The essential Blender: guide to 3D creation with the open source suite Blender*. No Starch Press, 2007. 4

[7] Haochen Huang, Jiahuan Pei, Mohammad Aliannejadi, Xin Sun, Moonisa Ahsan, Chuang Yu, Zhaochun Ren, Pablo Cesar, and Junxiao Wang. Lego co-builder: exploring fine-grained vision-language modeling for multimodal lego assembly assistants. *arXiv preprint arXiv:2507.05515*, 2025. 4

[8] Youngkyoon Jang, Brian Sullivan, Casimir Ludwig, Iain D. Gilchrist, Dima Damen, and Walterio Mayol-Cuevas. Epictent: An egocentric video dataset for camping tent assembly. In *2019 IEEE/CVF International Conference on Computer Vision Workshop (ICCVW)*, pages 4461–4469, 2019. 2

[9] L.E. Kavraki, P. Svestka, J.-C. Latombe, and M.H. Overmars. Probabilistic roadmaps for path planning in high-dimensional configuration spaces. *IEEE Transactions on Robotics and Automation*, 12(4):566–580, 1996. 3

[10] Maurice G Kendall. A new measure of rank correlation. *Biometrika*, 30(1-2):81–93, 1938. 6

[11] Mohammad Sadil Khan, Sankalp Sinha, Talha Uddin Sheikh, Didier Stricker, Sk Aziz Ali, and Muhammad Zeshan Afzal. Text2cad: Generating sequential cad designs from beginner-to-expert level text prompts. In *Advances in Neural Information Processing Systems*, pages 7552–7579. Curran Associates, Inc., 2024. 2

[12] Zachary Kingston, Mark Moll, and Lydia E. Kavraki. Sampling-based methods for motion planning with constraints. *Annual Review of Control, Robotics, and Autonomous Systems*, 1(Volume 1, 2018):159–185, 2018. 3

[13] H. W. Kuhn. The Hungarian method for the assignment problem. *Naval Research Logistics Quarterly*, 2(1-2):83–97, 1955. 5

[14] Steven M. LaValle. Rapidly-exploring random trees : a new tool for path planning. *The annual research report*, 1998. 3

[15] Jiahao Li, Weijian Ma, Xueyang Li, Yunzhong Lou, Guichun Zhou, and Xiangdong Zhou. CAD-Llama: Leveraging large language models for computer-aided design parametric 3d model generation. In *Proceedings of the IEEE/CVF Conference on Computer Vision and Pattern Recognition (CVPR)*, pages 18563–18573, 2025. 2

[16] Yichen Li, Kaichun Mo, Lin Shao, Minhyuk Sung, and Leonidas Guibas. Learning 3d part assembly from a single image. In *Computer Vision – ECCV 2020: 16th European Conference, Glasgow, UK, August 23–28, 2020, Proceedings, Part VI*, page 664–682, Berlin, Heidelberg, 2020. Springer-Verlag. 1, 3, 5, 6, 7

[17] Yulong Li, Andy Zeng, and Shuran Song. Rearrangement planning for general part assembly. In *Proceedings of The 7th Conference on Robot Learning*, pages 127–143. PMLR, 2023. 3, 7

[18] Yichen Li, Kaichun Mo, Yueqi Duan, He Wang, Jiequan Zhang, Lin Shao, Wojciech Matusik, and Leonidas Guibas. Category-level multi-part multi-joint 3D shape assembly. In *2024 IEEE/CVF Conference on Computer Vision and Pattern Recognition (CVPR)*, pages 3281–3291, 2024. 3

[19] Yunong Liu, Cristobal Eyzaguirre, Manling Li, Shubh Khanna, Juan Carlos Niebles, Vineeth Ravi, Saumitra Mishra, Weiyu Liu, and Jiajun Wu. IKEA manuals at work: 4d grounding of assembly instructions on internet videos. In *The Thirty-eight Conference on Neural Information Processing Systems Datasets and Benchmarks Track*, 2024. 2, 3, 4

[20] Yuxing Long, Jiyao Zhang, Mingjie Pan, Tianshu Wu, Taewhan Kim, and Hao Dong. CheckManual: A new challenge and benchmark for manual-based appliance manipulation. In *Proceedings of the IEEE/CVF Conference on Computer Vision and Pattern Recognition (CVPR)*, 2025. 2, 4

[21] Kaichun Mo, Shilin Zhu, Angel X. Chang, Li Yi, Subarna Tripathi, Leonidas J. Guibas, and Hao Su. PartNet: A large-scale benchmark for fine-grained and hierarchical part-level 3D object understanding. In *The IEEE Conference on Computer Vision and Pattern Recognition (CVPR)*, 2019. 2

[22] Newton Contributors. Newton: GPU-accelerated physics simulation for robotics, and simulation research., 2025. 2, 7

[23] Aaron van den Oord, Yazhe Li, and Oriol Vinyals. Representation learning with contrastive predictive coding. *arXiv preprint arXiv:1807.03748*, 2018. 6

[24] Mayank Patel, Rahul Jain, Asim Unmesh, and Karthik Ramani. Dynamo: Dependency-aware deep learning framework for articulated assembly motion prediction. *2509.12430*, 2025. 2

[25] Ava Pun, Kangle Deng, Ruixuan Liu, Deva Ramanan, Changliu Liu, and Jun-Yan Zhu. Generating physically stable and buildable brick structures from text. In *Proceedings of the IEEE/CVF International Conference on Computer Vision (ICCV)*, pages 14798–14809, 2025. 2

[26] Nadav Schor, Oren Katzir, Hao Zhang, and Daniel Cohen-Or. Componet: Learning to generate the unseen by part synthesis and composition. In *IEEE Proceedings of the International Conference on Computer Vision, (ICCV)*, pages 8758–8767. IEEE, 2019. Publisher Copyright: © 2019 IEEE.; 17th IEEE/CVF International Conference on Computer Vision, ICCV 2019 ; Conference date: 27-10-2019 Through 02-11-2019. 3

[27] Fadime Sener, Dibyadip Chatterjee, Daniel Shelepov, Kun He, Dipika Singhania, Robert Wang, and Angela Yao. Assembly101: A large-scale multi-view video dataset for understanding procedural activities. In *Proceedings of the IEEE/CVF Conference on Computer Vision and Pattern Recognition (CVPR)*, pages 21096–21106, 2022. 2

[28] Oriane Siméoni, Huy V Vo, Maximilian Seitzer, Federico Baldassarre, Maxime Oquab, Cijo Jose, Vasil Khalidov, Marc Szafraniec, Seungeun Yi, Michaël Ramamonjisoa, et al. Dinov3. *arXiv preprint arXiv:2508.10104*, 2025. 5

[29] Daniel Sliwowski, Shail Jadav, Sergej Stanovcic, Jedrzej Orbik, Johannes Heidersberger, and Dongheui Lee. Reassemble: A multimodal dataset for contact-rich robotic assembly and disassembly. *arXiv preprint arXiv:2502.05086*, 2025. 2

[30] Bingjie Tang, Iretiayo Akinola, Jie Xu, Bowen Wen, Ankur Handa, Karl Van Wyk, Dieter Fox, Gaurav S. Sukhatme, Fabio Ramos, and Yashraj Narang. Automate: Specialist and generalist assembly policies over diverse geometries. In *Robotics: Science and Systems*, 2024. 1

[31] Yunsheng Tian, Jie Xu, Yichen Li, Jieliang Luo, Shinjiro Sueda, Hui Li, Karl D.D. Willis, and Wojciech Matusik. Assemble them all: Physics-based planning for generalizable assembly by disassembly. *ACM Trans. Graph.*, 41(6), 2022. 2, 3, 4

[32] Yunsheng Tian, Karl DD Willis, Bassel Al Omari, Jieliang Luo, Pingchuan Ma, Yichen Li, Farhad Javid, Edward Gu, Joshua Jacob, Shinjiro Sueda, et al. Asap: Automated sequence planning for complex robotic assembly with physical feasibility. In *2024 IEEE International Conference on Robotics and Automation (ICRA)*, pages 4380–4386. IEEE, 2024. 2, 3, 4

[33] Yunsheng Tian, Joshua Jacob, Yijiang Huang, Jialiang Zhao, Edward Gu, Pingchuan Ma, Annan Zhang, Farhad Javid, Branden Romero, Sachin Chitta, et al. Fabrica: dual-arm assembly of general multi-part objects via integrated planning and learning. *arXiv preprint arXiv:2506.05168*, 2025. 1

[34] Chenrui Tie, Shengxiang Sun, Yudi Lin, Yanbo Wang, Zhongrui Li, Zhouhan Zhong, Jinxuan Zhu, Yiman Pang, Haonan Chen, Junting Chen, et al. Manual2Skill++: Connector-aware general robotic assembly from instruction manuals via vision-language models. *arXiv preprint arXiv:2510.16344*, 2025. 1, 2, 3, 4

[35] Chenrui Tie, Shengxiang Sun, Jinxuan Zhu, Yiwei Liu, Jingxiang Guo, Yue Hu, Haonan Chen, Junting Chen, Ruihai Wu, and Lin Shao. Manual2skill: Learning to read manuals and acquire robotic skills for furniture assembly using vision-language models. *arXiv preprint arXiv:2502.10090*, 2025. 1, 2, 3

[36] Ashish Vaswani, Noam Shazeer, Niki Parmar, Jakob Uszkoreit, Llion Jones, Aidan N Gomez, Łukasz Kaiser, and Illia Polosukhin. Attention is all you need. *Advances in neural information processing systems*, 30, 2017. 5

[37] Ruocheng Wang, Yunzhi Zhang, Jiayuan Mao, Chin-Yi Cheng, and Jiajun Wu. Translating a visual LEGO manual to a machine-executable plan. In *European Conference on Computer Vision (ECCV)*, pages 677–694. Springer Nature Switzerland, 2022. 2, 4

[38] Ruocheng Wang, Yunzhi Zhang, Jiayuan Mao, Ran Zhang, Chin-Yi Cheng, and Jiajun Wu. IKEA-Manual: Seeing shape assembly step by step. In *NeurIPS 2022 Datasets and Benchmarks Track*, 2022. 1, 2, 3, 4

[39] Rundi Wu, Yixin Zhuang, Kai Xu, Hao Zhang, and Baoquan Chen. PQ-NET: A generative part seq2seq network for 3d shapes. In *IEEE/CVF Conference on Computer Vision and Pattern Recognition (CVPR)*, 2020. 3

[40] Boshen Xu, Sipeng Zheng, and Qin Jin. SPAFormer: Sequential 3D part assembly with transformers. In *International Conference on 3D Vision (3DV)*, pages 1317–1327, 2025. 3

[41] Jingwei Xu, Chenyu Wang, Zibo Zhao, Wen Liu, Yi Ma, and Shenghua Gao. CAD-MLLM: Unifying multimodality-conditioned CAD generation with MLLM. *arXiv preprint arXiv:2411.04954*, 2024. 2

[42] Jiahao Zhang, Anoop Cherian, Yanbin Liu, Yizhak Ben-Shabat, Cristian Rodriguez, and Stephen Gould. Aligning step-by-step instructional diagrams to video demonstrations. In *Conference on Computer Vision and Pattern Recognition (CVPR)*, 2023. 2, 3

[43] Jiahao Zhang, Anoop Cherian, Cristian Rodriguez, Weijian Deng, and Stephen Gould. Manual-PA: Learning 3d part assembly from instruction diagrams. In *Proceedings of the IEEE/CVF International Conference on Computer Vision*, pages 6304–6314, 2025. 1, 2, 3, 4, 5, 6, 7, 8

[44] Yanzhao Zhang, Mingxin Li, Dingkun Long, Xin Zhang, Huan Lin, Baosong Yang, Pengjun Xie, An Yang, Dayiheng Liu, Junyang Lin, et al. Qwen3 embedding: Advancing text embedding and reranking through foundation models. *arXiv preprint arXiv:2506.05176*, 2025. 5

[45] Hao Zheng, Regina Lee, and Yuqian Lu. Ha-vid: a human assembly video dataset for comprehensive assembly knowledge understanding. In *Proceedings of the 37th International Conference on Neural Information Processing Systems*, Red Hook, NY, USA, 2023. Curran Associates Inc. 2

[46] Xinghao Zhu, Devesh K Jha, Diego Romeres, Lingfeng Sun, Masayoshi Tomizuka, and Anoop Cherian. Multi-level reasoning for robotic assembly: From sequence inference to contact selection. In *2024 IEEE international conference on robotics and automation (ICRA)*, pages 816–823. IEEE, 2024. 2, 3

AssemblyBench: Physics-Aware Assembly of Complex Industrial Objects –Supplementary Materials–

Danrui Li[1*] Jiahao Zhang[2*] Bernhard Egger[3]
Moitreya Chatterjee[4] Suhas Lohit[4] Tim K. Marks[4] Anoop Cherian[4]
[1]Rutgers, The State University of New Jersey, USA [2]The Australian National University, Australia
[3]Friedrich-Alexander-Universität Erlangen-Nürnberg, Germany [4]Mitsubishi Electric Research Laboratories (MERL), USA
[1]danrui.li@rutgers.edu [2]jiahao.zhang@anu.edu.au [3]bernhard.egger@fau.de [4]{chatterjee,slohit,tmarks,cherian}@merl.com

https://www.merl.com/research/highlights/assemblybench

Table of Contents

1. Detailed Performance Analysis

1.1. Effect of the Number of Steps

As shown in Figure 1, across both settings (GT order and Standard) and both metrics (PA, SR), all curves decline as the number-of-step bin increases, indicating that longer sequences, which contain more complex diagrams and assembled geometries, are harder. SR drops more steeply than PA and often approaches zero for long sequences under simulation, acting as the most strict metric in our study.

Meanwhile, it shows AssemblyDyno is more robust in simulation. In the simulation protocol (solid lines), *AssemblyDyno* (red) consistently lies above *ManualPA* (blue) for both PA and SR across nearly all number-of-step bins and in both settings, showing stronger execution robustness.

Again, the figure demonstrates our simulation is the stricter evaluation. For every method, metric, and setting, solid lines are lower than dashed lines (final-pose evaluation), confirming that simulation reveals failures that static end-state checks miss.

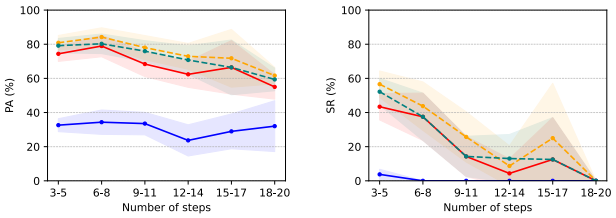

(a) GT order setting

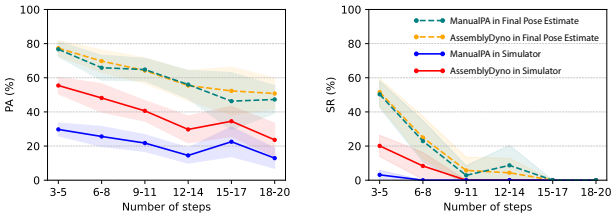

(b) Standard setting

Figure 1. **Performance as a function of number of steps**. We present the PA and SR metric in two evaluation protocols (static final pose and simulation), for AssemblyDyno and ManualPA in two experiment settings. Shaded areas represent 95% confidence intervals of the metric.

*Work done during internships at MERL.

1.2. Effect of Trajectory Category

We compare our work against the ManualPA baseline [3] across multiple trajectory categories and two evaluation settings. As shown in Table 1, both approaches perform well on stationary trajectories. Stationary trajectories are always the first step of the assembly, where both the context and motion are simple. In contrast, for complex motions such as rotational or insert-and-rotate trajectories, the performance of both methods drops, but our approach remains substantially more robust, achieving noticeably higher PA and lower geometric error. Overall, across most categories and in both settings, our method outperforms ManualPA, doubling the improvement in PA.

Table 1. **Comparison of assembly performance across trajectory categories.** For each category, we report three metrics computed using our simulation-based evaluation protocol: median Average Chamfer Distance (mACD), median Final Chamfer Distance (mFCD), and Percentage of Accurate assemblies (PA). We compare them against corresponding results from the baseline (*ManualPA*[3]).

Category	**mACD** (10^{-3})↓		**mFCD** (10^{-3})↓		**PA (%)**↑	
	Ours	[3]	Ours	[3]	Ours	[3]
Standard Setting						
All	**34.82**	192.79	**15.97**	56.04	**42.9**	23.2
Stationary	**5.92**	108.21	5.72	**4.41**	61.1	**62.9**
Translational	**33.73**	187.06	**15.36**	50.92	**43.8**	24.5
Rotational	**50.48**	272.77	**26.76**	159.05	**30.6**	5.6
Insertion	**147.83**	250.08	**10.15**	40.26	**48.8**	26.7
Insert + Rotate	206.59	**189.52**	**44.20**	82.64	**14.3**	0.0
GT Order Setting						
All	**9.97**	230.52	**4.43**	35.00	**70.1**	31.3
Stationary	**2.78**	120.48	2.72	**2.53**	**77.5**	76.4
Translational	**9.43**	224.32	**4.30**	30.25	**70.9**	33.1
Rotational	**14.49**	373.30	**7.21**	215.70	**59.7**	6.5
Insertion	**100.24**	288.18	**5.92**	40.24	**73.3**	34.9
Insert + Rotate	**117.38**	166.57	**10.36**	67.83	**42.9**	0.0

1.3. Effect of Loss Design

Ablation Study. From the ablation results in Table 2, we observe that all loss components in our framework are essential. Removing any individual loss term ($\mathcal{L}_P$, $\mathcal{L}_T$, $\mathcal{L}_R$, or $\mathcal{L}_{SR}$) consistently degrades performance across both the *Final Pose Estimate* metrics and the *Assembly in Simulator* metrics. The drops are particularly notable in the simulation-based metrics (mACD, mFCD, PA, and SR), indicating that each loss contributes critically to enabling the model to produce physically executable assembly trajectories. These observations confirm the necessity of the full loss design used in AssemblyDyno.

Sensitivity Analysis We further conduct a sensitivity analysis by varying the weights of the rotational loss λ_R and the rotation-regularization loss λ_{SR}. The original weights are in Table 4. Across the tested weight settings, the resulting performance metrics exhibit only small fluctuations. This low variance indicates that our method is robust to moderate perturbations of these hyperparameters. Thus, within the examined range, the overall assembly performance is not highly sensitive to the specific weight choices of these losses, demonstrating stability of the training objective.

1.4. Effect of Text Instructions

While the aggregated performance gains in Table 2 may appear marginal (+2%), the influence of text is not sufficiently unveiled. Specifically, for challenging assemblies such as the one in Fig. 2a, we find that incorporation of text leads to significant benefits. In Fig. 2b, we plot the median improvement in part-wise chamfer distance (CD) by AssemblyDyno, as a function of CD of the text-omitted version. Clearly, text instructions yield significant gains (up to 40%) for the worst cases ($\text{CD} > 10^{-2}$, the right half of the plot). This is currently not reflected in the PA metric we report, as it only counts the fraction of parts with $\text{CD} < 10^{-2}$. We will include this in the final paper.

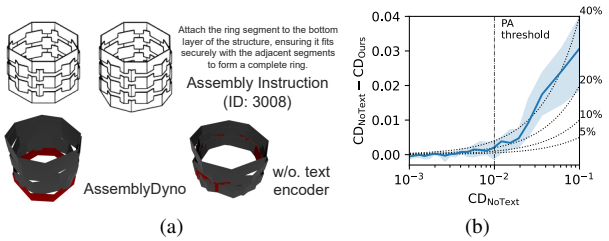

(a) (b)

Figure 2. Text helps for difficult cases. **(a)** Example instruction step (top) and resulting prediction with vs. without using text (bottom). **(b)** Median value of $\text{CD}_{\text{NoText}} - \text{CD}_{\text{Ours}}$, plotted vs. $\text{CD}_{\text{NoText}}$.

1.5. Adding Multiple Parts in One Step

To evaluate the robustness of our model when multiple parts are added in a single step, we trained and tested our model while randomly removing (masking) the diagrams for up to 2 steps from each assembly. Table 3 shows that our model is significantly more robust to missing step diagrams than the Manual-PA baseline.

2. Physics-aware or physics-in-the-loop?

In this paper, we use the term "physics-aware" to indicate that a physics engine is used to generate the ground-truth part trajectories in our dataset and to evaluate the assemblies predicted by models.

We attempted a "physics-in-the-loop" strategy for our model, where physics constraint signals are included in the training loss. However, we found it to be less effective than

Table 2. **Part assembly results on the test split of AssemblyBench**. Best results are in **bold**, second best in blue.

Model	Final Pose Estimate			Assembly in Simulator			
	SCD(10^{-3})↓	PA(%)↑	SR(%)↑	mACD(10^{-3})↓	mFCD(10^{-3})↓	PA(%)↑	SR(%)↑
AssemblyDyno	3.87	**79.69**	44.29	9.97	4.43	70.15	**33.57**
w/o $\mathcal{L}_P$	4.09	77.75	38.57	10.79	5.11	67.91	27.50
w/o $\mathcal{L}_T$	4.19	68.43	27.86	17.69	6.92	57.41	25.00
w/o $\mathcal{L}_R$	3.97	73.71	37.14	11.94	5.26	64.57	26.43
w/o $\mathcal{L}_{S_R}$	3.85	79.17	43.21	16.98	11.06	47.18	5.36
Sensitivity Analysis							
$\lambda_R = 1$	3.88	78.64	42.86	10.15	4.59	69.11	30.00
$\lambda_R = 10$	3.74	79.49	**46.43**	**9.16**	**4.24**	**70.20**	32.14
$\lambda_{S_R} = 1$	**3.71**	79.61	44.64	10.93	5.65	64.35	20.00
$\lambda_{S_R} = 10$	3.82	79.20	40.71	10.04	**4.24**	70.04	30.36

Table 3. When step diagrams are randomly masked out (keeping text), AssemblyDyno is much more robust than ManualPA.

Model	Masked?	SCD(10^{-3})↓	PA(%)↑	SR(%)↑
AssemblyDyno	-	3.81	77.08	40.36
	✓	**4.61**	**69.20**	**22.86**
ManualPA	-	4.15	77.40	39.28
	✓	6.02	60.90	9.286

supervised training using ground-truth assembly trajectories.

This claim is supported by experiments where we use simulator refinements at test time: when predicted final part poses exhibit even minor interpenetrations (on the order of mm), we use a physics simulator to resolve these by pushing parts apart, resulting in large displacements from the ground-truth poses (see Figure 3 left). Such refinements is detrimental, reducing PA from 79.69% to 70.53% and SR from 44.29% to 36.79%.

In Figure 3 right, we conceptually illustrate this difficulty using a hypothetical ground-truth part trajectory and the directions of collision-induced forces from the simulator. As shown, when ground-truth trajectories are available, they can provide substantially stronger and more stable learning signals than the noisy collision gradients from the simulator. Consequently, designing effective collision-aware losses or post-processing schemes would require significant innovations beyond the scope of this work.

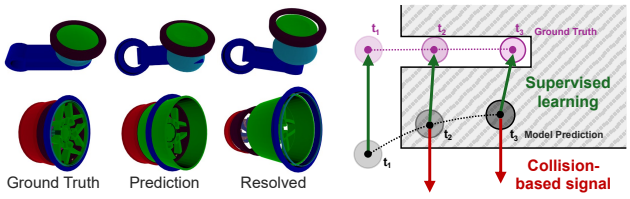

Figure 3. **Left**: Physics-based post-processing of an assembly. **Right**: Supervised learning guides predictions towards ground truth, while collision forces push parts to the nearest free space.

3. Physics Simulator Configurations

We present the most important simulator configurations in Table 5, which consists of general settings such as gravity and simulation substeps, as well as material settings that determined the friction behaviors of the shape. The friction parameters `kf` and `mu` need to be set to 0 in our evaluation. as shown in Figure 4, when friction effects are not disabled, some insertion behaviors will not be executed, even if we use ground truth trajectories to guide the simulator.

While we use a specific simulator [1] in our study, our evaluation protocol (*i.e.* the simulation design and its metrics) is agnostic to simulator choice, as long as it supports collision detections on non-convex mesh geometries.

Table 4. Hyperparameters for training AssemblyDyno.

Name	Value	Name	Value
Batch size	64	Epoch	1,000
Optimizer	AdamW	Learning rate	4×10^{-5}
Weight decay	1×10^{-4}	Betas for AdamW	$(0.9, 0.999)$
λ_P	20	λ_T	1
λ_R	20	λ_{S_T}	1
λ_{S_R}	20		

Table 5. **Simulator Configurations**. The most important parameters contain general settings (first two parameters) and material settings (the remaining). The parameters that differ from default simulator settings are **bolded**.

Parameter	Description	Value
`gravity`	The gravity force.	**0.0**
`substeps`	Substeps between trajectory waypoints.	60
`ka`	The contact adhesion distance.	0.0
`kd`	The contact damping stiffness.	1000.0
`ke`	The contact elastic stiffness.	100000.0
`kf`	The contact friction stiffness.	**0.0**
`mu`	The coefficient of friction.	**0.0**
`restitution`	The coefficient of restitution.	0.0
`thickness`	The thickness of the shape.	1e-05

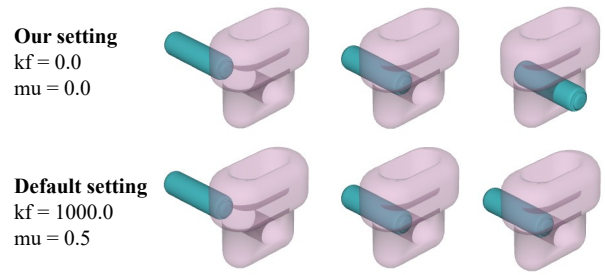

Figure 4. **Effects of Friction Parameters**. (Top) when disabling the friction effects in the simulator (our setting), the orange part can be successfully installed under the guidance of ground truth trajectory. (Bottom) default friction setting leads to a stuck at the rim of the hole.

4. Performance of Classic Motion Planning

We choose RRT and RRT-connect (used in [2]) to demonstrate classical motion planning methods are not suitable for the assembly trajectory generations in our scenario where the final poses are predicted. We conduct this experiment on a Windows Subsystem for Linux with an Intel Core i9-14900K CPU (32 cores) and 128 GB RAM.

In the following experiments, we feed the predicted final poses from AssemblyDyno to the two motion planning methods, instructing them to calculate the corresponding assembly motion. We inspect if they can provide solutions, no matter the quality, within given time constraints.

Table 6 highlights two major limitations of classical motion planners. First, these methods are inherently slow and struggle to find solutions under practical time constraints. Even with generous limits such as 30 s or 60 s, both RRT and RRT-Connect achieve success rates below 10%, indicating that they rarely return solutions quickly enough to be useful in real-world assembly scenarios.

More importantly, even when a very long time limit is imposed (120s), classical planners still fail to solve more than a small fraction of the tasks. This shows that classical planners require strictly collision-free goal states. However, the predicted final poses from AssemblyDyno may contain minor shape overlaps or small interpenetrations between parts, which are unavoidable when predictions are generated by learning-based models. These small inconsistencies cause classical planners to reject the goal configuration or become stuck while attempting to resolve infeasible collisions, preventing them from producing valid trajectories even with unlimited compute.

Assemble-them-all uses a search heuristic to produce part trajectories, whose computational complexity is combinatorial in the number of parts. While it takes 6.7s to produce assemblies on average, we found that tail cases take much longer, e.g., only 57.5% achieve success at $\leq 30s$.

Table 6. **Success rate of non-neural motion planning**. We present the success rate of returning answers (regardless of their quality) under varying time constraints. We use the predicted final poses from AssemblyDyno as inputs.

Algorithm	**Success Rate (%) with Timeout Constraints**						
	1s	2s	5s	10s	30s	60s	120s
RRT	2.9	3.6	4.6	5.0	6.4	6.8	7.1
RRT-Connect	2.9	3.2	3.6	4.6	5.4	6.1	7.1
Assemble Them All	4.6	8.6	21.8	34.6	57.5	72.1	81.8

Instead, our AssemblyDyno predicts all part trajectories *in a single forward pass*.

5. Qualitative Results

Figure 5 illustrates user-manual assembly instructions alongside our model's predicted trajectories. For each step, we visualize the motion as a sequence of temporally ordered point-cloud snapshots rendered as semi-transparent overlays. Although each trajectory contains 12 time steps, we display only the 1st, 6th, and 12th steps to provide a clear yet concise depiction of the object's motion during assembly. These overlaid time-step frames highlight how the predicted trajectories evolve over time and how the parts move toward their final configurations in each manual step.

6. Limitation

Unlike IKEA-style furniture parts, which often have significant part symmetries and duplications, the complex industrial parts in AssemblyBench (including large variation in part sizes) are found to be sensitive to even minor changes in the camera viewpoints. We believe new approaches for view-invariant diagram representations are necessary, and our multiview data generation pipeline facilitates research into this important topic.

7. Dataset Construction Details

7.1. User Study of the User Manuals

We conduct a two-stage user survey to evaluate the quality of our part names and text instructions. First, participants are shown 200 assembled CAD shapes, each with two rendered views and color-labeled parts, and are asked to count incorrectly named parts (*e.g.*, a cube labeled as "sphere"). As shown in Fig. 6, 72.9% of shapes contain zero incorrect names, and over 90% contain at most one or two, indicating high semantic accuracy.

Second, for each assembly we sample one instruction step and provide the current diagram, prior diagram, text instruction, and a labeled reference image. Participants rate text quality (1–10) and verify whether the spatial instruction

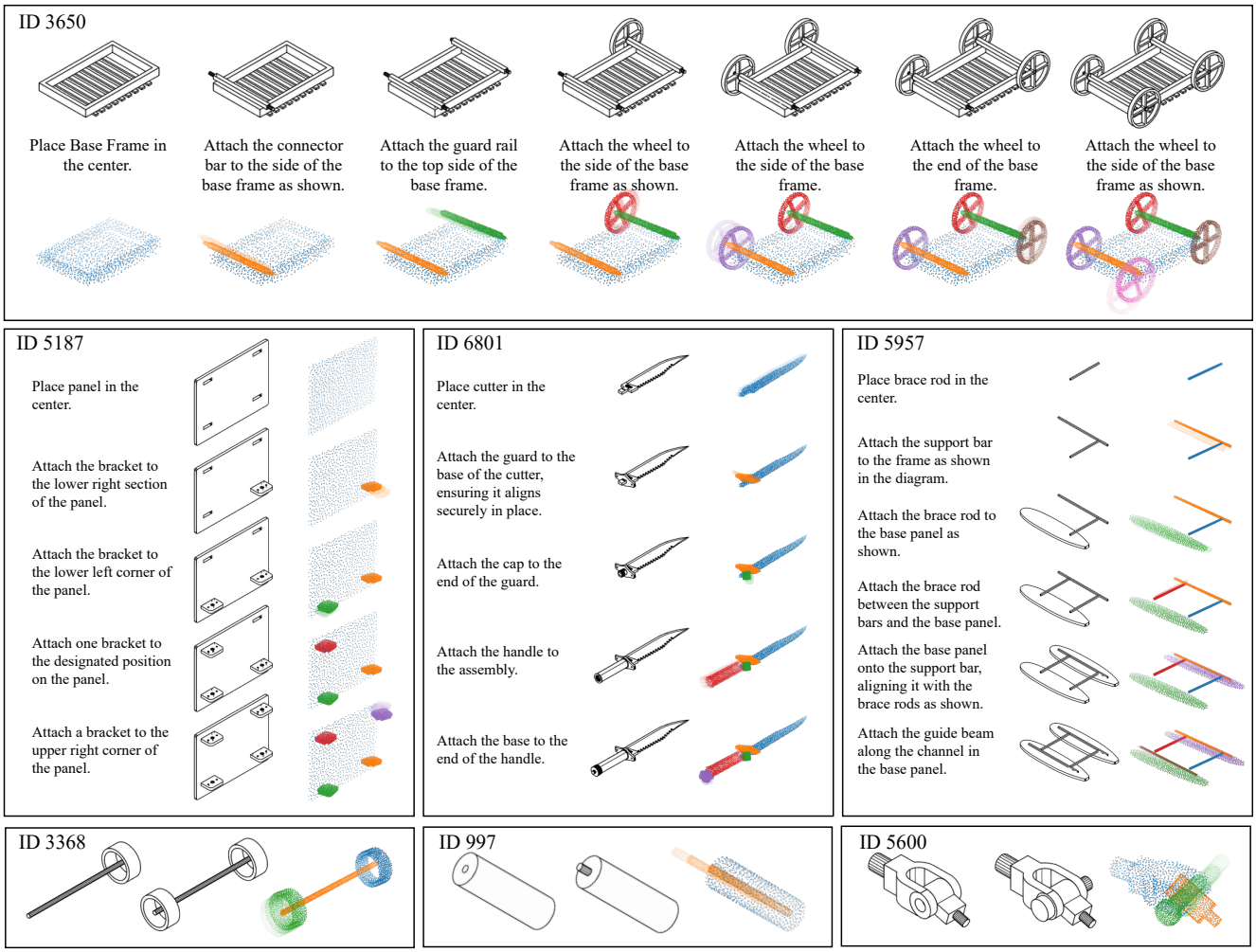

Figure 5. **User manuals with predicted trajectories**. We present the user manual and predicted trajectories of AssemblyDyno as the colored point clouds. Top two rows illustrate complete user manuals while the last row features insertion assembly steps. Multiple time steps are overlapped as transparent layers. The trajectories are executed in the stimulator, showing their outcomes when considering physical constraints.

matches the diagram. Results show that 54.1% of text instructions receive a rating of 10, and over two-thirds score 9 or above. Spatial correctness is also high: 91.4% of instructions are labeled correct. These outcomes confirm that our part names, textual descriptions, and spatial references are reliably annotated, providing a strong foundation for downstream tasks.

7.2. Choose Diagram Camera Views

As we render all diagrams in a set of camera views, for each shape assembly, We apply a heuristic to select the camera view that best demonstrate the assembly process. The objective is to choose, for each assembly part, a camera view that provides strong visual coverage of the part during the relevant assembly step and in the final assembled state. The method proceeds in three conceptual stages: (1) measur-

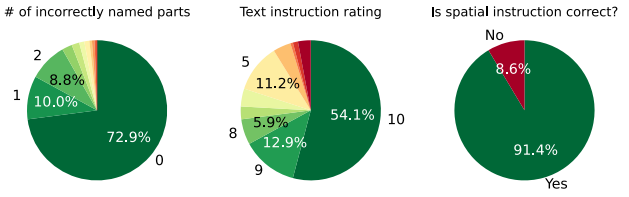

Figure 6. **User study on text annotation quality**. We present: (left) the distribution of incorrect part name amounts within a sampled assembly shape; (middle) the distribution of subjective text instruction ratings among all sampled shapes, higher is better; (right) the proportion of correct spatial information in the text instructions.

ing visibility, (2) scoring and normalizing per-part visibility, and (3) combining scores across the entire assembly to produce a consistent camera assignment.

Visibility Measurement Consider a set of cameras indexed by $c \in \mathcal{C}$, and a sequence of assembly parts indexed in order by $p \in \mathcal{P}$. For each camera c and part p, we observe two images:

- the diagram taken at the assembly step when part p is assembled, and
- the diagram taken at the final assembly completion.

From each diagram image we extract the number of pixels belonging to part p. Let $n_{c,p}^{(A)}$ and $n_{c,p}^{(F)}$ denote, respectively, the number of pixels of part p visible in camera c during the assembly step and during the final step. Thus, visibility is characterized by the pair $\left(n_{c,p}^{(A)},\ n_{c,p}^{(F)}\right)$.

Per-Part Visibility Score Visibility should contribute to the score in a way that has diminishing returns for large pixel counts. A logarithmic visibility score fulfills this requirement. For each camera c and part p, define:

$$s_{c,p} = \begin{cases} \log\left(1 + \lambda\, n_{c,p}^{(A)}\right) + \log\left(1 + \lambda\, n_{c,p}^{(F)}\right), & \text{if } n_{c,p}^{(A)} > 0, \\ 0, & \text{if } n_{c,p}^{(A)} = 0, \end{cases}$$

where λ is a scaling constant set as 0.05 that moderates the influence of raw pixel counts.

This construction ensures:

- both assembly-step visibility and final-step visibility contribute additively,
- visibility in the assembly step is essential (otherwise the score is zero),
- visibility contributions grow sublinearly.

For each part p, the visibility scores $\{s_{c,p}\}_{c\in\mathcal{C}}$ are divided by the max score across all cameras ($\max_{c\in\mathcal{C}} s_{c,p}$), so that the best camera attains a normalized score $\hat{s}_{c,p}$.

Aggregated Camera Quality Across All Parts To determine which cameras are most useful across the entire assembly process, the normalized per-part scores are summed over all parts to S_c.

$$S_c = \sum_{p\in\mathcal{P}} \hat{s}_{c,p}.$$

The quantity S_c expresses the overall usefulness of camera c across the entire assembly. The cameras are ranked in descending order of S_c. This global ranking reflects which cameras tend to provide good visibility for many parts.

7.3. Instructional Text Generation

We use VLMs to name the CAD parts one by one. For each CAD part, we provide the VLM with the following text prompts and three images:

- The diagram from the first step where the part is introduced, with the part highlighted.
- The final-step diagram of the completed assembly, also highlighting the same part.
- When there are similar parts in the assembly, we provide an additional diagram where all its counterparts are highlighted.

> You are a product design assistant who write user manuals.
> You should name the colored component in the first image.
> In the second image, you are given the final assembled model with your focus component colored.
> In the third image, all similar components are colored for your reference. You should give a general name (in singular form) for all these similar components.
>
> – Adopt one name. Don't include multiple choices.
> – Don't include color into names.
> – Avoid using oriental words such as left, right, horizontal.
> – Avoid existing part names: {existing_names}
>
> Think in steps and finalize your answer in json.
> Example output:
> ```
> json
> {
>   "name": "Feet"
> }
>
> json
> {
>   "name": "Connector Bar"
> }
> ```

We find similar parts by grouping their bounding box sizes. As we prompt the VLM to assign a general name for each group, we only name one part within the group.

For all diagrams, we choose the best camera view from a predefined set, by colorizing the target part and selecting the view that maximizes the number of colored pixels of our target part in the diagram image. The camera views vary among CAD parts, which is different from final user manuals, where all diagrams share the same view within the shape assembly.

We use the generated names to create text instructions for final user manuals. We generate assembly text instructions step-by-step. Within each VLM call, we provide the following text prompts with two images, where the camera views align with the final user manuals.:

- The diagram of the current assembly step, with the part to be assembled highlighted in color.
- The same diagram of the same step, but with all of the parts highlighted in varying colors and labeled by their names.

You are a product design assistant who write user manuals.
You should describe the assembly step of the first image, which involves only one component highlighted in color.
The names of the current component and previous components are shown in the second image as a reference.

– Just describe the current assembly step.
– Don't include instructions for previous steps and components.
– Correct the incorrect plural form of the component name if any.
– Don't subdivide the current step into multiple sub–steps.
– Avoid words like "as shown in the image" or "as illustrated".
– Don't include color in your description.

Think in steps and finalize your answer in json.
Example output:

```
json
{
  "text": "your description here"
}
```

References

[1] Newton Contributors. Newton: GPU-accelerated physics simulation for robotics, and simulation research., 2025. 3

[2] Chenrui Tie, Shengxiang Sun, Jinxuan Zhu, Yiwei Liu, Jingxiang Guo, Yue Hu, Haonan Chen, Junting Chen, Ruihai Wu, and Lin Shao. Manual2skill: Learning to read manuals and acquire robotic skills for furniture assembly using vision-language models. *arXiv preprint arXiv:2502.10090*, 2025. 4

[3] Jiahao Zhang, Anoop Cherian, Cristian Rodriguez, Weijian Deng, and Stephen Gould. Manual-PA: Learning 3d part assembly from instruction diagrams. In *Proceedings of the IEEE/CVF International Conference on Computer Vision*, pages 6304–6314, 2025. 2